eprints@whiterose.ac.uk
https://eprints.whiterose.ac.uk/

Disturbance-Rejection Position Tracking Control of Industrial Robots Via A Discrete-Time Super-Twisting-Observer-Based Fast Terminal Sliding Mode Approach

Linyan Han[1,4], Jianliang Mao[2,4], Haibo Du[3], Yahui Gan[4] and Shihua Li[4]

Abstract

Facing the system uncertainties caused by unmodeled dynamics and unpredictable external disturbances, the robot position control for meeting the high-performance control requirements on higher accuracy and faster beat is vital for many industrial applications, such as welding and laser cutting tasks. This work aims to cope with the problem of precise and fast position tracking for robot manipulators with an effective and safe control scheme. Specifically, a discrete-time super-twisting observer (STO) is integrated into the scheme to estimate the uncertain dynamics (e.g., unmodeled dynamics and external disturbances) in the feedforward compensation part of the dynamics. Subsequently, a discrete-time fast terminal sliding mode controller (FTSMC) dominates the robot control to guarantee fast convergence of the position tracking error. The significant improvement of the proposed method with respect to other discrete-time sliding mode control approaches lies in that it is capable of alleviating the chattering-like problem, achieving a fast convergence and improving the robustness of sliding mode control against uncertain dynamics. To illustrate the effectiveness of the presented control scheme, several experiments on a six-degree-of-freedom (6-DoF) robot manipulator are provided.

1 Introduction

In many manufacturing processes, industrial robots have a wide range of applications (e.g., welding Shen et al. (2020), polishing Xiao et al. (2021) and milling Peng et al. (2020) tasks). In order to improve production efficiency and quality and complete these tasks successfully, robots often need to be equipped with control algorithms with fast running beat and high tracking accuracy. However, the robotic system always encounters various uncertainties (e.g., the coupling among the links, unmodeled dynamics, parameter uncertainties), which may negatively affect the realization of high-speed and high-precision position tracking control. Hence, in order to achieve the requirements of robots in high-performance application scenarios, it is very important to restrain the effect of uncertainties from the perspective of controller design.

In practice, the suffered disturbances of robotic systems are very complex, which can be deemed as the main factor that affects the high-performance control of robots. The sources of such disturbances can be divided into internal disturbances (e.g., unmodeled dynamics and parameter uncertainties) and external disturbances (e.g., unknown load disturbances). It is commonly accepted that the accuracy of conventional approaches (such as the PD plus gravity compensation approach and the computational torque method) is significantly affected by dynamic uncertainties in high-speed operations. In light of the reliable robustness against disturbances and uncertainties Utkin (2013), the well-known sliding mode control (SMC) has achieved much attention in a wide range of applied research Wang et al. (2018), Tang et al. (2021). Meanwhile, a multitude of state-of-the-art achievements can be explored in the community of SMC, ranging from asymptotic Utkin (1977) to finite-time Mao et al. (2020), low-order Yu and Kaynak (2009) to high-order Ozer et al. (2018), and continuous-time Norsahperi and Danapalasingam (2020) to discrete-time Paul et al. (2019) approaches. In addition, due to the improvement of modern computer technology, the modern nonlinear controller is actually realized by the digital microprogrammed control units in practice. Therefore, this work attempts to solve these problems by developing a control scheme based on the discrete-time SMC works.

In general, the discrete-time SMC mainly falls into two major categories. The first one primarily concentrates on the reaching-law theory Zhang et al. (2018), which is similar to the continuous-time SMC and inherits the nature of its switching terms, making

[1]School of Mechanical Engineering, University of Leeds, Leeds LS2 9JT, UK
[2]College of Automation Engineering, Shanghai University of Electric Power, Shanghai 200090, PR China
[3]School of Electrical Engineering and Automation, Hefei University of Technology, Hefei, 230009, China
[4]School of Automation, Southeast University, Key Laboratory of Measurement and Control of Complex Systems of Engineering, Ministry of Education, Nanjing 210096, PR China

Corresponding author:
Shihua Li, School of Automation, Southeast University, Nanjing 210096, PR China.
Email: lsh@seu.edu.cn

the chattering problem inevitable. In a real robotic system, such chattering causes the wear between the actuator and the transmission mechanism, and will further induce the unmodeled high-frequency dynamics. Another category to design the discrete-time SMC is the equivalent-control-based approaches proposed in Abidi et al. (2008), Du et al. (2016), Li et al. (2013), whereas the chattering problem can be obviously alleviated. Recently, the digital FTSMC, inheriting the key benefits of the linear sliding mode controller (LSMC) and the terminal sliding mode controller (TSMC) Wang et al. (2017), Liu et al. (2020), has been redesigned in Du et al. (2018) and widely used in the field of motion control Wang et al. (2020). In these works, however, the disturbances are treated by using the delayed estimation method (DEM), which mainly use the past value of the disturbance to approximate the disturbance at the current moment Su et al. (2000). In fact, this method, which is equivalent to the finite-difference method, relies on the acceleration signal, thereby amplifies the noises easily in practice Zhang et al. (2019). In view of this, the method based on the discrete-time observer techniques can be employed as an effective manner to smooth the measurements and estimate the unknown disturbances. Until now, several discrete-time observer techniques have been developed in various scenarios, such as discrete-time disturbance observer Yan et al. (2023) and discrete-time STO Salgado et al. (2014).

Inspired by the aforementioned background, the purpose of this paper is to develop a discretized STO-based FTSMC scheme for facilitating robotic manipulators to fast and accurately track desired trajectories. Then, experiments are conducted with a real 6-DoF industrial robot, validating that the developed scheme can achieve reliable performance under various disturbances. In particular, the main contributions of this article are listed below:

(i) *A discrete-time STO is proposed to estimate dynamic uncertainties, and the bound of the estimation error is built through rigorous theoretical analysis, differing from the previous DEM works which are limited to measurement noises. Moreover, the observation information is integrated for the feedforward compensation, thus not only improving the robustness of the system, but also reducing chattering to some extent.*

(ii) *An improved composite controller is proposed for industrial robots by incorporating the estimations of the STO into a discrete-time FTSMC for realizing high-speed and high-precision position tracking, which is an essential advantage of using this composite controller in improving the robot beat and control precision. To the best of our knowledge, most of the existing robot dynamics control methods are still in the simulation stage.*

Notations: For an n-dimensional vector $\mathbf{x} = \left[x_1, x_2, \ldots, x_n\right]^{\mathrm{T}}$, the vectors $|\mathbf{x}| = \left[|x_1|, |x_2|, \ldots, |x_n|\right]^{\mathrm{T}}$, $\mathrm{sign}(\mathbf{x}) = \left[\mathrm{sign}(x_1), \mathrm{sign}(x_2), \ldots, \mathrm{sign}(x_n)\right]^{\mathrm{T}}$, $\mathrm{diag}(\mathbf{x}^{\alpha}) = \mathrm{diag}(x_1^{\alpha}, x_2^{\alpha}, \ldots, x_n^{\alpha})$. $\|\cdot\|$ denotes Euclidean norm of vectors. $\lambda_{\max}(\cdot)$ and $\lambda_{\min}(\cdot)$ correspond to the maximum and minimum eigenvalues of a matrix, respectively. $\mathrm{sig}^{\alpha}(\mathbf{x}) = \left[|x_1|^{\alpha}\mathrm{sign}(x_1), |x_2|^{\alpha}\mathrm{sign}(x_2), \ldots, |x_n|^{\alpha}\mathrm{sign}(x_n)\right]^{\mathrm{T}}$ are defined associated with the positive constant $\alpha > 0$. $\mathcal{O}$ represents that $f(h)$ is said to be of order $g(h)$ and

can be described as $f(h) = \mathcal{O}(g(h))$, if exists $\delta > 0$ and $A > 0$ so that $|f(h)| < A|g(h)|$ for $|h| < \delta$.

2 Problem formulation

Formally, the typical dynamic equation of n-link robot manipulators is illustrated as

$$\mathbf{M}(\mathbf{q})\ddot{\mathbf{q}} + \mathbf{C}(\mathbf{q}, \dot{\mathbf{q}}) + \mathbf{g}(\mathbf{q}) = \tau + \tau_d \tag{1}$$

where $\mathbf{q}$, $\dot{\mathbf{q}}$, $\ddot{\mathbf{q}}$ respectively correspond to n-dimensional vectors of joint position, velocity and acceleration, while n is the number of motion freedom degrees of robot manipulators. $\mathbf{M}(\mathbf{q})$ is a $n \times n$ symmetric, positive-definite matrix, $\mathbf{C}(\mathbf{q}, \dot{\mathbf{q}})$ is the $n \times 1$ vector of Coriolis and centrifugal terms, $\mathbf{g}(\mathbf{q})$ is the $n \times 1$ gravity force, τ denotes the $n \times 1$ vector of control input and τ_d represents unknown external disturbances.

Defining $\mathbf{x}_1 = \mathbf{q}$, $\mathbf{x}_2 = \dot{\mathbf{q}}$ and based on (1), we can obtain

$$\begin{aligned} \dot{\mathbf{x}}_1 &= \mathbf{x}_2 \\ \dot{\mathbf{x}}_2 &= \mathbf{M}^{-1}(\mathbf{x}_1)\tau + \mathbf{f} + \mathbf{d} \end{aligned} \tag{2}$$

with the $\mathbf{d} \in \mathbb{R}^n$ defined as follows

$$\mathbf{d} = \mathbf{M}^{-1}(\mathbf{x}_1)\tau_d \tag{3}$$

and

$$\mathbf{f} = -\mathbf{M}^{-1}(\mathbf{x}_1)\left(\mathbf{C}(\mathbf{x}_1, \mathbf{x}_2) + \mathbf{g}(\mathbf{x}_1)\right). \tag{4}$$

Since the modern nonlinear controller is realized by the digital microprogrammed control units, we here exploit the Euler-Discrete method to discretize the dynamic model (2) in order to promote the design of a discrete-time control law. Note that the control objective of this paper is to track the reference trajectory accurately by the proposed digital controller, which is executed via a zero-order-holder (ZOH) so as to control laws $\tau(t)$ equal to $\tau(kh)$ over the time interval $[kh, (k+1)h)$ with $k \in \{0, 1, 2, \dots, \} = \mathcal{Z}^+ \cup \{0\}$. From the perspective of information transmission, there is an error between the approximated discrete-time model and the continuous-time model, but considering the high real-time performance of industrial robots, the error here can be ignored. Formally, the corresponding discretization model of system (2) is

$$\begin{aligned} \mathbf{x}_1(k+1) &= \mathbf{x}_1(k) + h\mathbf{x}_2(k) \\ \mathbf{x}_2(k+1) &= \mathbf{x}_2(k) + h\left(\mathbf{M}^{-1}(\mathbf{x}_1)\tau(k) + \mathbf{f}(k) + \mathbf{d}(k)\right) \end{aligned} \tag{5}$$

where h denotes the sampling period. Meanwhile, for sake of simplicity, $\mathbf{x}_i(k)$ denotes the state $\mathbf{x}_i(kh)$ with $i = 1, 2$.

Define position tracking errors as $\mathbf{e}_1 = \mathbf{x}_r - \mathbf{x}_1$, $\mathbf{e}_2 = \dot{\mathbf{x}}_r - \mathbf{x}_2$, where $\mathbf{x}_r$ and $\dot{\mathbf{x}}_r$ represent the reference position and velocity, respectively. Then, considering (2), the

error dynamics can be governed by

$$\begin{aligned}
\dot{\mathbf{e}}_1 &= \mathbf{e}_2 \\
\dot{\mathbf{e}}_2 &= \ddot{\mathbf{x}}_r - \mathbf{M}^{-1}(\mathbf{x}_1)\tau - \mathbf{f} - \mathbf{d}.
\end{aligned} \tag{6}$$

Using the Euler-Discrete method again, the error system (6) can be discretized as

$$\begin{aligned}
\mathbf{e}_1(k+1) &= \mathbf{e}_1(k) + h\mathbf{e}_2(k) \\
\mathbf{e}_2(k+1) &= \mathbf{e}_2(k) + h\ddot{\mathbf{x}}_r(k) - h\mathbf{M}^{-1}(\mathbf{x}_1)\tau(k) - h\mathbf{f}(k) - h\mathbf{d}(k).
\end{aligned} \tag{7}$$

Furthermore, the following technical lemmas and the assumption on the disturbances are central to derive the main results, as shown below.

Lemma 1: Du et al. (2015) For the following system

$$\xi(k+1) = \xi(k) - \iota_1 \mathrm{sig}^\alpha \xi(k) - \iota_2 \xi(k) + \chi(k) \tag{8}$$

with $0 < \alpha < 1$, $\iota_1 > 0$, $0 < \iota_2 < 1$, if $|\chi(k)| \le \nu$, $\nu > 0$, then the system state $\xi(k)$ is always bounded and there exist a finite number $N^* > 0$ such that

$$|\xi(k)| \le \Phi(\alpha) \cdot \max\left\{ \left(\frac{\nu}{\iota_1}\right)^{1/\alpha}, \left(\frac{\iota_1}{1-\iota_2}\right)^{\frac{1}{1-\alpha}} \right\}, \forall k \ge N^* \tag{9}$$

with $\Phi(\alpha)$ is determined as

$$\Phi(\alpha) = 1 + \alpha^{\frac{\alpha}{1-\alpha}} - \alpha^{\frac{1}{1-\alpha}}. \tag{10}$$

Lemma 2: Li et al. (2013) Consider the following scalar system

$$\xi(k+1) = \xi(k) - \iota \cdot \xi(k) + \chi(k). \tag{11}$$

If $|\iota| < 1$ and $|\chi(k)| < \nu$, $\nu > 0$, then the system state $\xi(k)$ is always bounded and there exist a finite number $N^* > 0$ such as $|\xi(k)| \le \frac{\nu}{|\iota|}$, $\forall k > N^*$.

Assumption 1: The disturbance $\mathbf{d}$ and its derivative $\dot{\mathbf{d}}$ satisfy these conditions, i.e., $\|\mathbf{d}\| \le d_0^*$ and $\|\dot{\mathbf{d}}\| \le d_1^*$, where d_0^* and d_1^* are two positive constants.

Remark 1: Consider that $\|\mathbf{M}^{-1}(\mathbf{x}_1)\|$ is bounded with $a_1 \le \|\mathbf{M}^{-1}(\mathbf{x}_1)\| \le a_2$, where a_1 and a_2 are two known positive constants Spong and Vidyasagar (1989). In addition, external disturbance signals τ_d can be reasonably assumed to be bounded. Hence, from the aforementioned analysis, it is reasonable to assume that $\|\mathbf{d}\|$ is bounded with a positive constant. According to assumption 1, due to $\delta(k) \triangleq \mathbf{d}(k) - \mathbf{d}(k-1) = \mathcal{O}(h)$, we can conclude that $\|\delta(k)\| \le \beta = \mathcal{O}(h)$ holds for any possible k, with $\beta = hd_1^*$.

3 Main results

Here, we propose to show the design process of the proposed control method, where a discrete-time super-twisting observer is first designed, and, subsequently, the estimated information is incorporated to derive the discrete-time FTSMC.

3.1 Discrete-time super-twisting observer

The discrete-time STO is proposed for estimating the disturbances in (5) (i.e., $\mathbf{d}(k)$), designed by

$$
\begin{aligned}
\mathbf{z}_2(k+1) &= \mathbf{z}_2(k) + h\left(\mathbf{f}(k) + \mathbf{M}^{-1}(\mathbf{x}_1)\tau(k) + \mathbf{z}_3(k)\right) \\
&\quad + h\mathbf{L}_1\mathrm{sig}^{\frac{1}{2}}(\mathbf{x}_2(k) - \mathbf{z}_2(k)) + \mathbf{L}_3(\mathbf{x}_2(k) - \mathbf{z}_2(k)) \\
\mathbf{z}_3(k+1) &= z_3(k) + h\mathbf{L}_2\mathrm{sign}(\mathbf{x}_2(k) - \mathbf{z}_2(k)) + \mathbf{L}_4(\mathbf{x}_2(k) - \mathbf{z}_2(k))
\end{aligned}
\tag{12}
$$

where $\mathbf{z}_2(k)$ and $\mathbf{z}_3(k)$ respectively correspond to the estimation of $\mathbf{x}_2(k)$ and $\mathbf{d}(k)$. $\mathbf{L}_i = \mathbf{L}_i^{\mathrm{T}} > \mathbf{0}$ for $i = 1, 2, 3, 4$ are the designed parameter matrices.

Define estimation errors as $\tilde{\mathbf{x}}_2(k) = \mathbf{x}_2(k) - \mathbf{z}_2(k)$, $\tilde{\mathbf{x}}_3(k) = \mathbf{d}(k) - \mathbf{z}_3(k)$ and $\tilde{\mathbf{x}}(k) = \begin{bmatrix} \tilde{\mathbf{x}}_2^{\mathrm{T}}(k) & \tilde{\mathbf{x}}_3^{\mathrm{T}}(k) \end{bmatrix}^{\mathrm{T}}$. Next, based on (5) and (12), one can obtain

$$
\tilde{\mathbf{x}}(k+1) = \mathbf{A}\tilde{\mathbf{x}}(k) + \mathbf{B}\mathrm{sign}(\tilde{\mathbf{x}}_2(k)) + \mathbf{\Delta}
\tag{13}
$$

where

$$
\mathbf{A} = \begin{bmatrix} \mathbf{I}_n - \mathbf{L}_3 & h\mathbf{I}_n \\ -\mathbf{L}_4 & \mathbf{I}_n \end{bmatrix}, \mathbf{B} = \begin{bmatrix} -h\mathbf{L}_1\mathbf{b}(k) \\ -h\mathbf{L}_2 \end{bmatrix}
$$

$$
\mathbf{\Delta} = \begin{bmatrix} \mathbf{0} \\ \delta(k+1) \end{bmatrix}, \mathbf{b}(k) = \mathrm{diag}(|\tilde{\mathbf{x}}_2(k)|^{\frac{1}{2}}).
$$

Theorem 1: According to Assumption 1, consider the robotic system (5) with gains chosen as $\mathbf{L}_i = \mathbf{L}_i^{\mathrm{T}} > \mathbf{0}$, $i = 1, 2, 3, 4$. If the parameters $\mathbf{L}_i$, $i = 1, 2, 3, 4$ and ρ are designed such that $|\lambda_{\max}(\mathbf{A})|/\sqrt{1-\rho} < 1$, the following inequality

$$
\mathbf{A}^{\mathrm{T}}\big(\mathbf{P} + \mathbf{P}(\mathbf{\Lambda}_1 + \mathbf{\Lambda}_2)\mathbf{P}\big)\mathbf{A} - (1-\rho)\mathbf{P} + \mathbf{Q} \leq \mathbf{0}
\tag{14}
$$

always has a positive definite solution $\mathbf{P} = \mathbf{P}^{\mathrm{T}} > \mathbf{0}$ for a given $\mathbf{Q} = \mathbf{Q}^{\mathrm{T}} > \mathbf{0}$, $\mathbf{\Lambda}_1 = \mathbf{\Lambda}_1^{\mathrm{T}} > \mathbf{0}$ and $\mathbf{\Lambda}_2 = \mathbf{\Lambda}_2^{\mathrm{T}} > \mathbf{0}$. Then, the estimation error of discrete-time STO is ultimately bounded by $\Omega = \{\tilde{\mathbf{x}}(k) \mid \|\tilde{\mathbf{x}}(k)\| \leq \eta_1\}$ with $\eta_1 = \sqrt{\frac{\beta_5}{\lambda_{\min}(\mathbf{P})\rho}}$, $0 < \rho < 1$, $\beta_5 = \frac{\beta_1^2}{4\beta_4} + \beta_2 + \beta_3\beta^2$, $\beta_1 = 2n^{\frac{3}{2}}h^2\lambda_{\max}(\mathbf{H}_1)\lambda_{\max}(\mathbf{L}_1^2)$, $\beta_2 = 2n^2h^2\lambda_{\max}(\mathbf{H}_1)\lambda_{\max}(\mathbf{L}_2^2)$, $\beta_3 = \lambda_{\max}(\mathbf{H}_2), \beta_4 = \lambda_{\min}(\mathbf{Q})$, $\mathbf{H}_1 = \mathbf{P} + \mathbf{\Lambda}_1^{-1} + \mathbf{\Lambda}_3$, $\mathbf{H}_2 = \mathbf{P} + \mathbf{\Lambda}_2^{-1} + \mathbf{P}\mathbf{\Lambda}_3^{-1}\mathbf{P}$, $\mathbf{\Lambda}_3 = \mathbf{\Lambda}_3^{\mathrm{T}} > \mathbf{0}$.

Proof: Select the following function similar to a Lyapunov one $V(k) = \tilde{\mathbf{x}}^{\mathrm{T}}(k)\mathbf{P}\tilde{\mathbf{x}}(k)$. Subsequently, we have

$$
\begin{aligned}
\Delta V(k) &= \tilde{\mathbf{x}}^{\mathrm{T}}(k+1)\mathbf{P}\tilde{\mathbf{x}}(k+1) - \tilde{\mathbf{x}}^{\mathrm{T}}(k)\mathbf{P}\tilde{\mathbf{x}}(k) \\
&= \tilde{\mathbf{x}}^{\mathrm{T}}(k)(\mathbf{A}^{\mathrm{T}}\mathbf{P}\mathbf{A} - \mathbf{P})\tilde{\mathbf{x}}(k) + 2\tilde{\mathbf{x}}^{\mathrm{T}}(k)\mathbf{A}^{\mathrm{T}}\mathbf{P}\mathbf{B}\mathrm{sign}(\tilde{\mathbf{x}}_2(k)) \\
&\quad + \mathrm{sign}(\tilde{\mathbf{x}}_2(k))^{\mathrm{T}}\mathbf{B}^{\mathrm{T}}\mathbf{P}\mathbf{B}\mathrm{sign}(\tilde{\mathbf{x}}_2(k)) + 2\tilde{\mathbf{x}}^{\mathrm{T}}(k)\mathbf{A}^{\mathrm{T}}\mathbf{P}\mathbf{\Delta} \\
&\quad + 2\mathbf{\Delta}^{\mathrm{T}}\mathbf{P}\mathbf{B}\mathrm{sign}(\tilde{\mathbf{x}}_2(k)) + \mathbf{\Delta}^{\mathrm{T}}\mathbf{P}\mathbf{\Delta}.
\end{aligned}
\tag{15}
$$

Due to the inequality $\mathbf{X}^{\mathrm{T}}\mathbf{Y} + \mathbf{Y}^{\mathrm{T}}\mathbf{X} \leq \mathbf{X}^{\mathrm{T}}\boldsymbol{\Lambda}^{-1}\mathbf{X} + \mathbf{Y}^{\mathrm{T}}\boldsymbol{\Lambda}\mathbf{Y}$ Poznyak (2010), the following relationships can be obtained

$$2\tilde{\mathbf{x}}^{\mathrm{T}}(k)\mathbf{A}^{\mathrm{T}}\mathbf{P}\mathbf{B}\mathrm{sign}(\tilde{\mathbf{x}}_2(k)) \leq \tilde{\mathbf{x}}^{\mathrm{T}}(k)\mathbf{A}^{\mathrm{T}}\mathbf{P}\boldsymbol{\Lambda}_1\mathbf{P}\mathbf{A}\tilde{\mathbf{x}}(k)$$
$$+ \mathrm{sign}(\tilde{\mathbf{x}}_2(k))^{\mathrm{T}}\mathbf{B}^{\mathrm{T}}\boldsymbol{\Lambda}_1^{-1}\mathbf{B}\mathrm{sign}(\tilde{\mathbf{x}}_2(k)), \qquad (16a)$$

$$2\tilde{\mathbf{x}}^{\mathrm{T}}(k)\mathbf{A}^{\mathrm{T}}\mathbf{P}\boldsymbol{\Delta} \leq \tilde{\mathbf{x}}^{\mathrm{T}}(k)\mathbf{A}^{\mathrm{T}}\mathbf{P}\boldsymbol{\Lambda}_2\mathbf{P}\mathbf{A}\tilde{\mathbf{x}}(k) + \boldsymbol{\Delta}^{\mathrm{T}}\boldsymbol{\Lambda}_2^{-1}\boldsymbol{\Delta}, \qquad (16b)$$

$$2\boldsymbol{\Delta}^{\mathrm{T}}\mathbf{P}\mathbf{B}\mathrm{sign}(\tilde{\mathbf{x}}_2(k)) \leq \boldsymbol{\Delta}^{\mathrm{T}}\mathbf{P}\boldsymbol{\Lambda}_3^{-1}\mathbf{P}\boldsymbol{\Delta} + \mathrm{sign}(\tilde{\mathbf{x}}_2(k))^{\mathrm{T}}\mathbf{B}^{\mathrm{T}}\boldsymbol{\Lambda}_3\mathbf{B}\mathrm{sign}(\tilde{\mathbf{x}}_2(k)). \qquad (16c)$$

If $|\lambda_{\max}(\mathbf{A})|/\sqrt{1-\rho} < 1$, the inequality described in (14) always has positive definite solution $\mathbf{P}^{\mathrm{T}} = \mathbf{P} > 0$. For the detailed proof, please refer to Salgado et al. (2014). Hence, we have $\mathbf{A}^{\mathrm{T}}\big(\mathbf{P} + \mathbf{P}(\boldsymbol{\Lambda}_1 + \boldsymbol{\Lambda}_2)\mathbf{P}\big)\mathbf{A} - (1-\rho)\mathbf{P} \leq -\mathbf{Q}$. Then substituting (16a)-(16c) into (15), $\triangle V(k)$ becomes

$$\begin{aligned}
\Delta V(k) &\leq \tilde{\mathbf{x}}^{\mathrm{T}}(k)\big(\mathbf{A}^{\mathrm{T}}\big(\mathbf{P} + \mathbf{P}(\boldsymbol{\Lambda}_1 + \boldsymbol{\Lambda}_2)\mathbf{P}\big)\mathbf{A} - (1-\rho)\mathbf{P}\big)\tilde{\mathbf{x}}(k) \\
&\quad - \rho V(k) + \mathrm{sign}(\tilde{\mathbf{x}}_2(k))^{\mathrm{T}}\mathbf{B}^{\mathrm{T}}\mathbf{H}_1\mathbf{B}\mathrm{sign}(\tilde{\mathbf{x}}_2(k)) + \boldsymbol{\Delta}^{\mathrm{T}}\mathbf{H}_2\boldsymbol{\Delta} \\
&\leq \tilde{\mathbf{x}}^{\mathrm{T}}(k)\big(\mathbf{A}^{\mathrm{T}}\big(\mathbf{P} + \mathbf{P}(\boldsymbol{\Lambda}_1 + \boldsymbol{\Lambda}_2)\mathbf{P}\big)\mathbf{A} - (1-\rho)\mathbf{P}\big)\tilde{\mathbf{x}}(k) \\
&\quad - \rho V(k) + \beta_1\|\tilde{\mathbf{x}}(k)\| + \beta_2 + \beta_3\beta^2 \\
&\leq -\tilde{\mathbf{x}}^{\mathrm{T}}(k)\mathbf{Q}\tilde{\mathbf{x}}(k) - \rho V(k) + \beta_1\|\tilde{\mathbf{x}}(k)\| + \beta_2 + \beta_3\beta^2 \\
&\leq -\beta_4\|\tilde{\mathbf{x}}(k)\|^2 - \rho V(k) + \beta_1\|\tilde{\mathbf{x}}(k)\| + \beta_2 + \beta_3\beta^2 \\
&= -\beta_4(\|\tilde{\mathbf{x}}(k)\| - \frac{\beta_1}{2\beta_4})^2 + \frac{\beta_1^2}{4\beta_4} + \beta_2 + \beta_3\beta^2 - \rho V(k) \\
&\leq -\rho V(k) + \beta_5.
\end{aligned} \qquad (17)$$

Then, one has

$$V(k+1) \leq (1-\rho)V(k) + \beta_5 \qquad (18)$$

whose solution corresponds to

$$V(k) \leq (1-\rho)^k V(0) + \sum_{i=0}^{k-1}(1-\rho)^{k-i-1}\beta_5$$
$$\leq (1-\rho)^k V(0) + \frac{1-(1-\rho)^k}{\rho}\beta_5. \qquad (19)$$

When k goes to infinity, (19) becomes

$$V(k) \leq \frac{\beta_5}{\rho} \qquad (20)$$

and we can conclude that the estimation error of the discrete-time STO is ultimately bounded by Ω. This result completes the proof. ∎

3.2 Discrete-time FTSMC

In this subsection, we aim to develop a digital control scheme that provides a fast response and has the anti-disturbance ability.

In accordance with the discrete-time robotic model (7), a nonlinear sliding mode surface can be constructed as

$$\mathbf{s}(k) = \mathbf{e}_2(k) + \mathbf{C}_1\mathbf{e}_1(k) + \mathbf{C}_2 sig^\alpha (\mathbf{e}_1(k)) \tag{21}$$

where c_{1i} is the ith element of diagonal matrix $\mathbf{C}_1 = \text{diag}(c_{11}, c_{12}, \ldots, c_{1n})$, requiring to be designed and satisfying $0 < hc_{1i} < 1$. $\mathbf{C}_2 = \text{diag}(c_{21}, c_{22}, \ldots, c_{2n})$ corresponds to a diagonal positive definite matrix to be designed and $0 < \alpha < 1$.

Subsequently, the equivalent control can be determined from the condition Su et al. (2000)

$$\mathbf{s}(k+1) = \mathbf{0}. \tag{22}$$

Substituting (7) into (22) yields

$$\mathbf{e}_2(k) + h\ddot{\mathbf{x}}_r(k) - h\mathbf{M}^{-1}(\mathbf{x}_1)\tau(k) - h\mathbf{f}(k) - h\mathbf{d}(k) + \mathbf{C}_1\mathbf{e}_1(k) \\ + h\mathbf{C}_1\mathbf{e}_2(k) + \mathbf{C}_2 sig^\alpha (\mathbf{e}_1(k+1)) = 0. \tag{23}$$

By substituting the estimated disturbance value (12) into (23), the discrete-time FTSMC is formulated as

$$\tau(k) = \underbrace{\frac{\mathbf{M}(\mathbf{x}_1)}{h}\left[(h\mathbf{C}_1 + \mathbf{I})\mathbf{e}_2(k) + \mathbf{C}_1\mathbf{e}_1(k)\right] + \frac{\mathbf{M}(\mathbf{x}_1)}{h}\left[\mathbf{C}_2 sig^\alpha (\mathbf{e}_1(k) + h\mathbf{e}_2(k))\right]}_{\tau_{fb}(k)}$$

$$+ \underbrace{\frac{\mathbf{M}(\mathbf{x}_1)}{h}\left[h\ddot{\mathbf{x}}_r(k) - h\mathbf{f}(k) - h\mathbf{z}_3(k)\right]}_{\tau_{ff}(k)}. \tag{24}$$

The proposed control law (24) consists of a feedforward part $\tau_{ff}(k)$ and a feedback part $\tau_{fb}(k)$. The disturbance estimation information $\mathbf{z}_3(k)$ in the feedforward not only compensates the disturbances but also mitigates chattering without sacrificing robustness. The non-smooth term $sig^\alpha(\cdot)$ in the feedback improves the dynamic response of the system state near the equilibrium points.

3.3 Stability analysis

In this subsection, the stability analysis for the case of (24) is presented. The detailed proof is shown as follows.

Theorem 2: Consider the discrete-time error dynamics (7) with the proposed discrete-time FTSMC consisting of the discrete-time STO (12), the sliding mode surface (21) and the control law (24). If Assumption 1 holds, then the position tracking error $\mathbf{e}_1(k)$ is ultimately bounded and has an accuracy with $\mathcal{O}(h^3)$ when $\alpha = \frac{2}{3}$.

Proof: We can apply (7), (21) and (24) to describe the dynamical behavior of $\mathbf{s}(k)$ as

$$
\begin{aligned}
\mathbf{s}(k+1) &= \mathbf{e}_2(k+1) + \mathbf{C}_1\mathbf{e}_1(k+1) + \mathbf{C}_2\mathrm{sig}^\alpha\left(\mathbf{e}_1(k+1)\right) \\
&= -h\left(\mathbf{d}(k) - \mathbf{z}_3(k)\right) \\
&= -h\tilde{\mathbf{x}}_3(k)
\end{aligned}
\tag{25}
$$

which is bounded by

$$
\begin{aligned}
|\mathbf{s}_i(k)| &\le \|\mathbf{s}(k)\| \le h\eta_1 = \mathcal{O}(h^2) \\
&\forall k \in \mathcal{Z}^+, \forall i \in \{1, 2, \ldots, n\}.
\end{aligned}
\tag{26}
$$

Thus, we can explain that $\mathbf{s}_i(k)$ has an $\mathcal{O}(h^2)$ boundary layer.

Recall that we have defined the discrete-time error dynamics in (7) and $\mathbf{e}_2(k)$ in (21), and thus the dynamical behavior of $\mathbf{e}_1(k)$ becomes

$$
\begin{aligned}
\mathbf{e}_1(k+1) &= h\left(\mathbf{s}(k) - \mathbf{C}_1\mathbf{e}_1(k) - \mathbf{C}_2\mathrm{sig}^\alpha\left(\mathbf{e}_1(k)\right)\right) + \mathbf{e}_1(k) \\
&= (\mathbf{I} - h\mathbf{C}_1)\,\mathbf{e}_1(k) + h\mathbf{s}(k) - h\mathbf{C}_2\mathrm{sig}^\alpha\left(\mathbf{e}_1(k)\right).
\end{aligned}
\tag{27}
$$

In accordance with Lemma 1, one can conclude that $\mathbf{e}_1(k)$ is always bounded. From (21), we have

$$
\mathbf{e}_2(k) = \mathbf{s}(k) - \mathbf{C}_1\mathbf{e}_1(k) - \mathbf{C}_2\mathrm{sig}^\alpha\left(\mathbf{e}_1(k)\right).
\tag{28}
$$

It is noted that $\mathbf{e}_2(k)$ depends on both terms $\mathbf{e}_1(k)$ and $\mathbf{s}(k)$ which are bounded based on the previous conclusions. Hence, one can conclude that the $\mathbf{e}_2(k)$ is also bounded, which further indicates that the stability of the closed-loop system can be ensured.

Then, by following Lemma 1, we have

$$
\begin{aligned}
|e_{1i}(\infty)| \le \rho_1 &= \Phi(\alpha) \cdot \max\left\{ \left(\frac{h^2\eta_1}{hc_{2i}}\right)^{\frac{1}{\alpha}}, \left(\frac{hc_{2i}}{1 - hc_{1i}}\right)^{\frac{1}{1-\alpha}} \right\} \\
&= \Phi(\alpha) \cdot \max\left\{ \left(\frac{h\eta_1}{c_{2i}}\right)^{\frac{1}{\alpha}}, \left(\frac{hc_{2i}}{1 - hc_{1i}}\right)^{\frac{1}{1-\alpha}} \right\} \\
&= \Phi(\alpha) \cdot \max\left\{ (\mathcal{O}(h))^{\frac{2}{\alpha}}, (\mathcal{O}(h))^{\frac{1}{1-\alpha}} \right\}, \\
&\forall k \ge N^*, \forall i \in \{1, 2, \ldots, n\}.
\end{aligned}
\tag{29}
$$

To obtain the optimal accuracy for $\mathbf{e}_1(k)$, select $\alpha = \frac{2}{3}$ such that

$$
2/\alpha = \frac{1}{1-\alpha}
\tag{30}
$$

holds. Hence,

$$
|e_{1i}(\infty)| \le \rho_1 = \mathcal{O}(h^3).
\tag{31}
$$

This completes the proof. ∎

Up to now, we have explained the stability of the proposed control method, which is related to both the structure of sliding mode surface and the steady state of sliding mode

state. We take advantage of this observation to derive our proposed method by formulate a novel sliding mode surface so as to achieve better control performance. Note that if $\alpha = 1$, the sliding surface described in (21) is transformed into a typical linear sliding surface, which fails to offer the fast transient convergence near the equilibrium point compared with the nonlinear sliding mode surface (21).

(a)

(b)
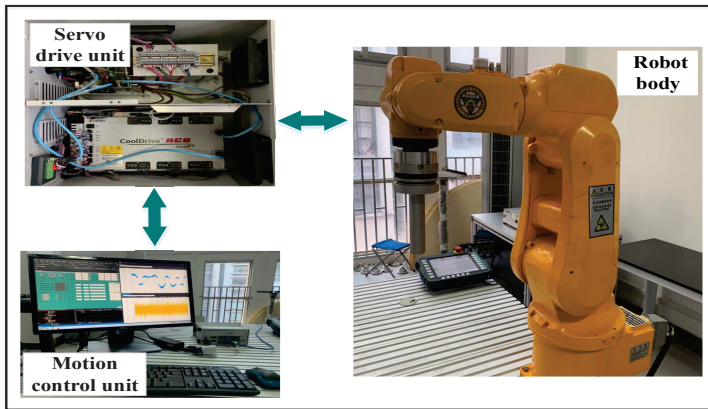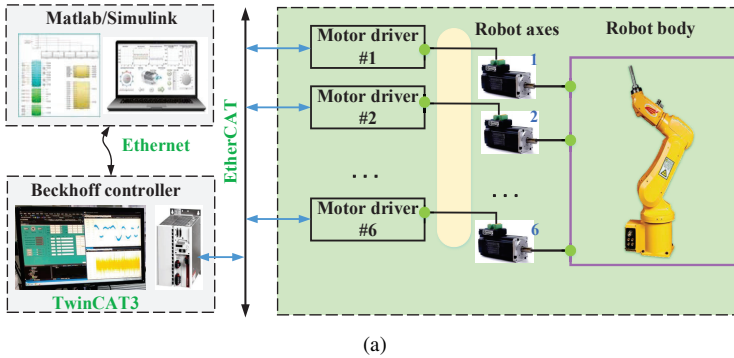
Figure 1. Experiment platform. (a) Overall design of the robot system. (b) Robotic arm system hardware diagram.

4 Experimental studies

This section presents several experimental evaluations to validate the performance of the proposed control method. The experimental platform is described in Figure 1. Please refer to Han et al. (2022) for details on this setup.

To show the control performance of our method, the discrete-time STO-based FTSMC (STO-FTSMC), comparisons with the discrete-time DEM-based FTSMC

Table 1. Control gains used on the robot

Controllers	Parameters
STO-FTSMC	$\mathbf{L}_1 = 10^2 \times \mathrm{diag}\{3,3,3,3,3,3\}$ $\mathbf{L}_2 = 10^4 \times \mathrm{diag}\{4.4, 4.4, 4.4, 4.4, 4.4, 4.4\}$ $\mathbf{L}_3 = \mathrm{diag}\{0.3, 0.3, 0.3, 0.3, 0.3, 0.3\}$ $\mathbf{L}_4 = \mathrm{diag}\{30, 30, 30, 30, 30, 30\}$ $\mathbf{C}_1 = 10^2 \times \mathrm{diag}\{4, 4, 4, 4, 4, 4\}$ $\mathbf{C}_2 = \mathrm{diag}\{30, 30, 30, 30, 30, 30\}$ $\alpha = \frac{2}{3}$
STO-LSMC	$\mathbf{L}_1 = 10^2 \times \mathrm{diag}\{3,3,3,3,3,3\}$ $\mathbf{L}_2 = 10^4 \times \mathrm{diag}\{4.4, 4.4, 4.4, 4.4, 4.4, 4.4\}$ $\mathbf{L}_3 = \mathrm{diag}\{0.3, 0.3, 0.3, 0.3, 0.3, 0.3\}$ $\mathbf{L}_4 = \mathrm{diag}\{30, 30, 30, 30, 30, 30\}$ $\mathbf{C}_1 = \mathrm{diag}\{430, 430, 320, 220, 220, 220\}$
DEM-FTSMC	$\mathbf{C}_1 = 10^2 \times \mathrm{diag}\{4, 4, 4, 4, 4\}$ $\mathbf{C}_2 = \mathrm{diag}\{30, 30, 30, 30, 30\}$ $\alpha = \frac{2}{3}$

(DEM-FTSMC) and STO-based LSMC (STO-LSMC) are provided. The DEM-FTSMC can be achieved by incorporating the output of DEM into the FTSMC, where the DEM is employed to estimate the disturbances that is designed as

$$
\begin{aligned}
\mathbf{z}_3(k) &= \mathbf{d}(k-1) \\
&= -\frac{1}{h}\left(\mathbf{e}_2(k) - \mathbf{e}_2(k-1)\right) + \ddot{\mathbf{x}}_r(k-1) - \mathbf{f}(k-1) - \mathbf{M}^{-1}(\mathbf{x}_1)\tau(k-1).
\end{aligned}
\tag{32}
$$

The discrete-time STO-LSMC is provided here. More details about its control design are as follows. The traditional linear discrete-time sliding surface is described as

$$
\mathbf{s}(k) = \mathbf{e}_2(k) + \mathbf{C}_1\mathbf{e}_1(k)
\tag{33}
$$

where c_{1i} is the ith element of diagonal matrix $\mathbf{C}_1 = \mathrm{diag}\left(c_{11}, c_{12}, \ldots, c_{1n}\right)$, requiring to be designed and satisfying $0 < hc_{1i} < 1$. Similar to the treatment in (22), we employ the equivalent control method to directly calculate the linear discrete-time SMC law. In addition, since the disturbance information is not yet available, we here exploit the same disturbance estimation treatment in (12) to obtain it. Subsequently, the final linear discrete-time SMC law associated with disturbances compensated can be derived as

$$
\begin{aligned}
\tau(k) &= \frac{\mathbf{M}(\mathbf{x}_1)}{h}\left[(h\mathbf{C}_1 + \mathbf{I})\mathbf{e}_2(k) + \mathbf{C}_1\mathbf{e}_1(k)\right] \\
&\quad + \frac{\mathbf{M}(\mathbf{x}_1)}{h}\left[h\ddot{\mathbf{x}}_r(k) - h\mathbf{f}(k) - h\mathbf{z}_3(k)\right].
\end{aligned}
\tag{34}
$$

On the basis of Lemma 2, we can derive that $\mathbf{e}_1(k)$ is bounded and its steady state will be bounded by

$$
|e_{1i}(\infty)| \leq \frac{h|s_i(\infty)|}{hc_{1i}} = \frac{h\eta_1}{c_{1i}} = \mathcal{O}(h^2), \forall i \in \{1, 2, \ldots, n\}.
\tag{35}
$$

Therefore, one can derive that $\mathbf{e}_1(k)$ has an accuracy with $\mathcal{O}(h^2)$.

The selection of control parameters is significant for control performance of robotic systems. The parameters $\mathbf{L}_i, i = 1, 2, 3, 4$ of the discrete-time STO need to be first
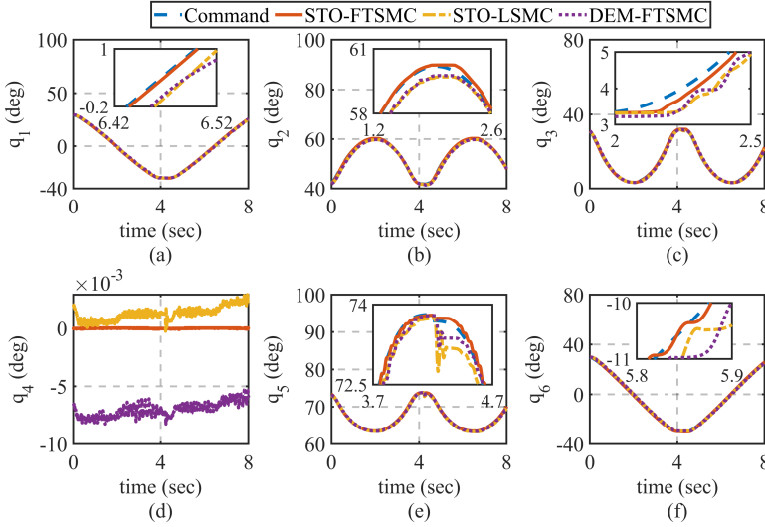
Figure 2. Comparison of the response curves for tracking the commanded position trajectory among the STO-FTSMC, STO-LSMC and DEM-FTSMC. $(a)-(f)$ respectively correspond to the first to sixth joints.

determined since the observer provides information for the controller design. Then, for parameter α, the condition (30) should be satisfied to obtain the optimal accuracy of $\mathbf{e}_1(k)$, and therefore α is set as $\frac{2}{3}$ in the experiment. Last, use the trial-and-error approach to set the parameters $\mathbf{C}_1$ and $\mathbf{C}_2$. The comparison with DEM-FTSMC and STO-LSMC are performed. For fair comparison purposes, we reuse the trial-and-error approach to adjust the control parameters until satisfactory tracking performance is achieved. The relevant parameters of the implemented controllers are listed in Table 1. Moreover, the sampling period h is set to 0.001 seconds.

Case I-Tracking performance under the commanded position trajectory.

In this test, we study a tracking task, where the robot is required to track commanded joint trajectories determined by the Jacobin-based inverse kinematics, which is aimed at evaluating the tracking performance of the above methods. We can observe that STO-FTSMC indeed has higher tracking accuracy, comparing with the DEM-FTSMC and STO-LSMC, as shown in Figure 2. Figure 3 shows the different disturbance estimation results through the discrete-time STO and DEM, where $\hat{\tau}_d = \mathbf{M}(\mathbf{x}_1)\hat{\mathbf{d}}$. It can be seen that the discrete-time STO performs better on disturbance estimation, unlike the DEM that brings some problems such as noise amplification and peaking phenomenon. Figure 4 depicts the response curves for control inputs via three methods.

Case II-Robustness against the unknown load disturbances.

The anti-disturbance performance of the control system is further studied in this experiment. In many robotic tasks, such as transportation and grasping tasks, robots are required to manipulate an unknown object to achieve a goal state. During this process,
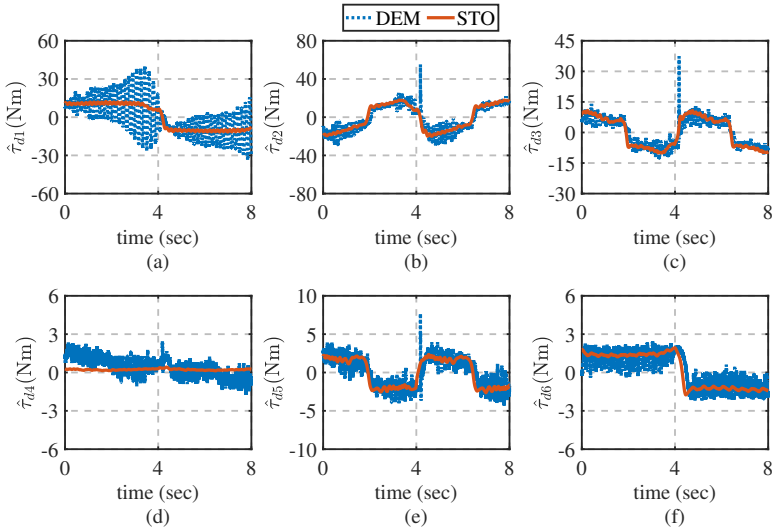
Figure 3. Disturbance estimation results through STO and DEM under tracking commanded position trajectories. $(a)-(f)$ correspond to the first to sixth joints.
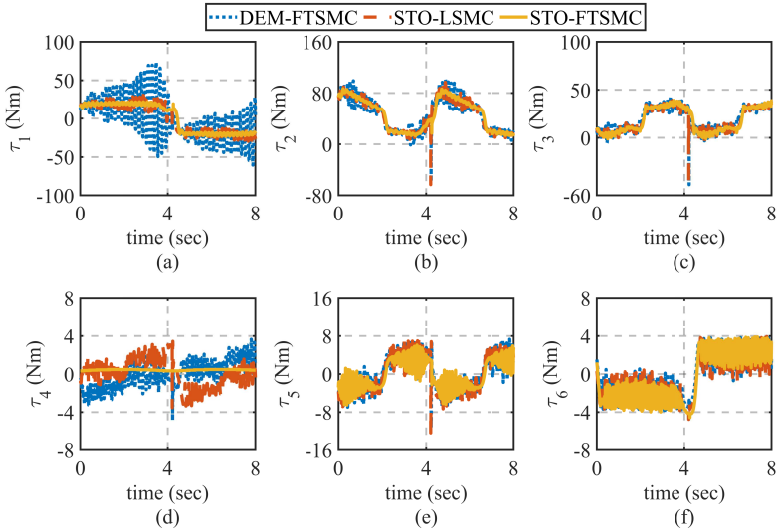
Figure 4. Control inputs of three approaches on tracking commanded position trajectories. $(a)-(f)$ correspond to the first to sixth joints.

the anti-disturbance ability plays a critical role in coping with the abrupt unknown load disturbances at the quasi-static state.
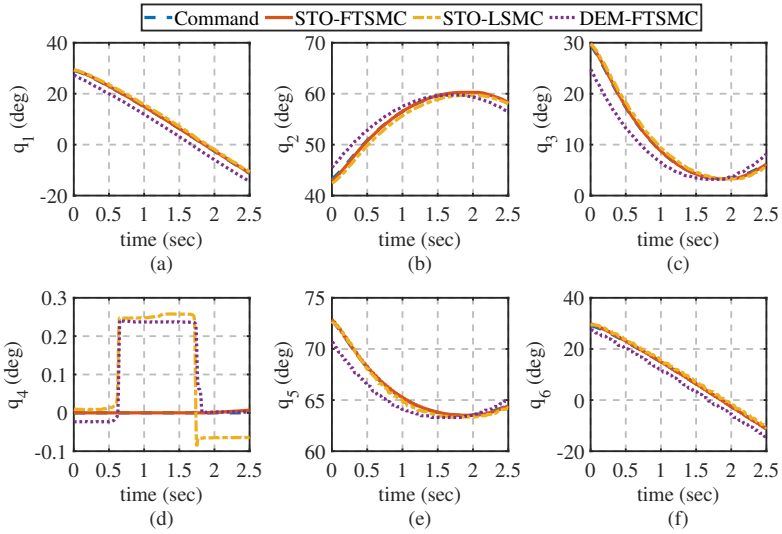
Figure 5. The response curves for position tracking via discrete-time STO-FTSMC and STO-LSMC as well as DEM-FTSMC under the unknown load disturbances. $(a)-(f)$ respectively correspond to the first to sixth joints.
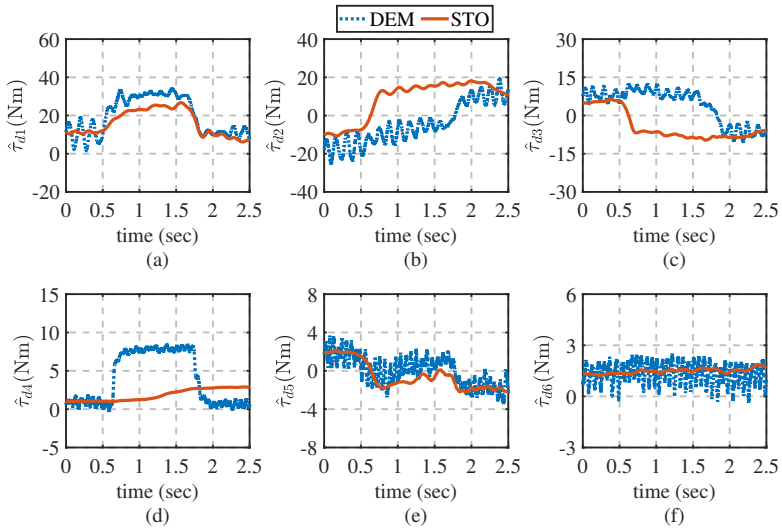
Figure 6. The estimated load disturbance via discrete-time STO and DEM. $(a)-(f)$ correspond to the first to sixth joints.
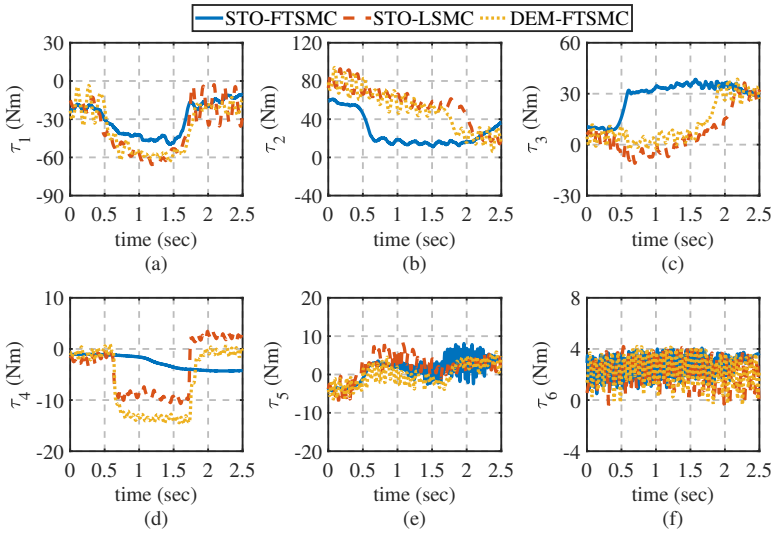
Figure 7. Control inputs of three approaches under unknown load disturbances. $(a)-(f)$ correspond to the first to sixth joints.
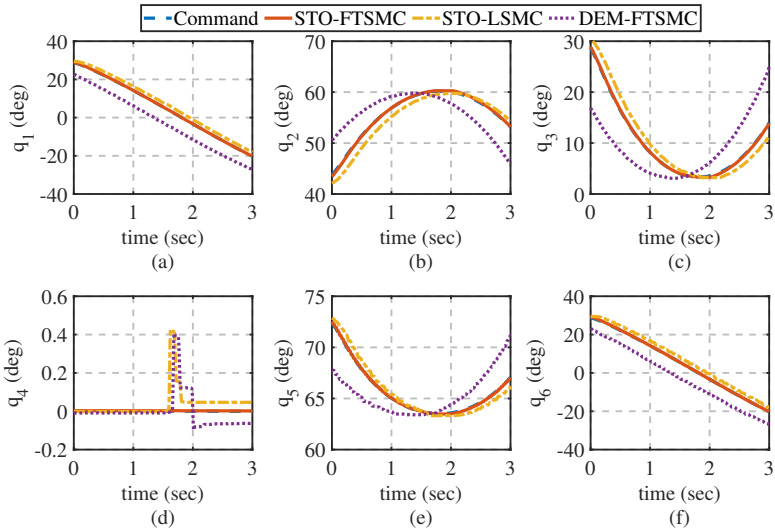
Figure 8. The response curves for position tracking via discrete-time STO-FTSMC, STO-LSMC and DEM-FTSMC under abrupt changes in disturbance. $(a)-(f)$ respectively correspond to the first to sixth joints.
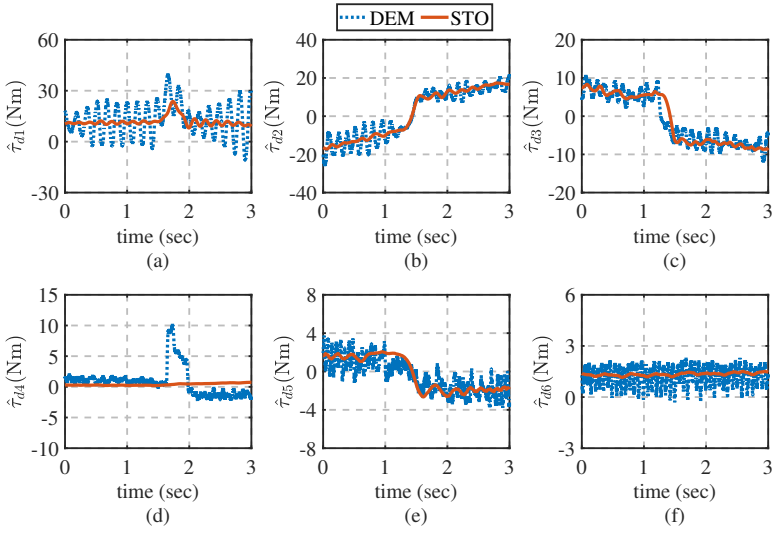
Figure 9. The estimated abrupt external disturbance via discrete-time STO and DEM. $(a)-(f)$ correspond to the first to sixth joints.
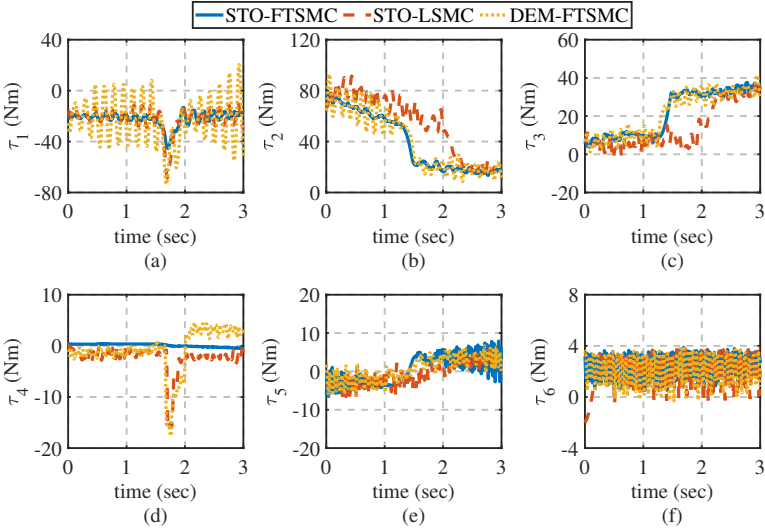
Figure 10. Control inputs of three approaches under abrupt changes in disturbance. $(a)-(f)$ correspond to the first to sixth joints.

An unknown load disturbance is imposed at the end-effector of the robot. As shown in Figure 5, we can observe that the proposed control method still exhibits better anti-disturbance capabilities. As shown in Figure 6, the discrete-time STO can effectively

Table 2. Performance Indexes Under Three Control Approaches In Case I.

	Joint 1 (deg)			Joint 2 (deg)		
	MAXE	MAE	STDE	MAXE	MAE	STDE
STO-FTSMC	0.2338	0.0606	0.0862	0.4076	0.1313	0.1640
STO-LSMC	0.3072	0.1150	0.1234	0.5874	0.3228	0.3619
DEM-FTSMC	0.5327	0.1479	0.1873	0.5660	0.3131	0.3366
	Joint 3 (deg)			Joint 4 (deg)		
	MAXE	MAE	STDE	MAXE	MAE	STDE
STO-FTSMC	0.3588	0.1258	0.1550	0.0001	0.00001	0.00002
STO-LSMC	0.5963	0.2970	0.3268	0.0029	0.0013	0.0014
DEM-FTSMC	0.6419	0.2149	0.2554	0.0083	0.0070	0.0070
	Joint 5 (deg)			Joint 6 (deg)		
	MAXE	MAE	STDE	MAXE	MAE	STDE
STO-FTSMC	0.1745	0.0557	0.0677	0.7136	0.1329	0.1954
STO-LSMC	0.6316	0.1318	0.1512	0.8735	0.4099	0.4576
DEM-FTSMC	0.4709	0.0979	0.1179	0.7525	0.3290	0.3772

estimate the unknown load disturbance. Figure 7 depicts the response curves for the control inputs under the unknown load disturbance.

Case III-Robustness against abrupt changes of the load.

In this test, we consider to abruptly impose an external force at the end-effector of the robot to verify the effectiveness of the proposed algorithm. In Figure 8, we can observe that the proposed method indeed is able to achieve better robustness against the abrupt changes in disturbance. The response curves of disturbance estimation and control inputs in joint space are shown in Figures 9 and 10, respectively.

In order to further quantitatively evaluate the proposed method, we consider the performance indexes such as MAXE, MAE and STDE (see Du et al. (2018) for details). For clear comparison results, the corresponding values with prescribed performance indexes are displayed closely in Table 2, which explicitly shows that the proposed control method is capable of providing better control performances than the other two methods.

5 Conclusions

In this paper, a robust discrete-time STO-FTSMC has been developed to achieve high-performance control requirements for industrial robots, where the disturbance compensation is considered. On the basis of the performed experimental tests on a real 6-DoF industrial robot, it shows that the proposed method can achieve the design requirements in the face of the uncertain dynamics and the unknown load disturbances as well as the abrupt changes in disturbance. Compared with the discrete-time STO-LSMC and DEM-FTSMC, the developed scheme improves the control performance on the position tracking accuracy and robustness. Besides, a strict theoretical analysis also validates the stability of this scheme by proving that the tracking error is ultimately bounded, which is also confirmed by the provided experimental results.

Acknowledgements

Declaration of conflicting interest

The authors declared no potential conflicts of interest with respect to the research, authorship, and/or publication of this article.

Funding

References

Abidi K, Xu J and She J (2008) A discrete-time terminal sliding-mode control approach applied to a motion control problem. *IEEE Transactions on Industrial Electronics* 56(9): 3619–3627.

Du H, Chen X, Wen G, Yu X and Lü J (2018) Discrete-time fast terminal sliding mode control for permanent magnet linear motor. *IEEE Transactions on Industrial Electronics* 65(12): 9916–9927.

Du H, Yu X, Chen M and Li S (2016) Chattering-free discrete-time sliding mode control. *Automatica* 68: 87–91.

Du H, Yu X and Li S (2015) *Recent Advances in Sliding Modes: From Control to Intelligent Mechatronics*. Springer.

Han L, Mao J, Cao P, Gan Y and Li S (2022) Towards sensorless interaction force estimation for industrial robots using high-order finite-time observers. *IEEE Transactions on Industrial Electronics* 69(7): 7275–7284.

Li S, Du H and Yu X (2013) Discrete-time terminal sliding mode control systems based on Euler's discretization. *IEEE Transactions on Automatic Control* 59(2): 546–552.

Liu W, Feng Z and Bi A (2020) A novel nonsingular terminal sliding mode control combined with global sliding surface for uncertain nonlinear second-order systems. *Transactions of the Institute of Measurement and Control* 42(7): 1294–1300.

Mao J, Yang J, Liu X, Li S and Li Q (2020) Modeling and robust continuous TSM control for an inertially stabilized platform with couplings. *IEEE Transactions on Control Systems Technology* 28(6): 2548–2555.

Norsahperi N and Danapalasingam K (2020) An improved optimal integral sliding mode control for uncertain robotic manipulators with reduced tracking error, chattering, and energy consumption. *Mechanical Systems and Signal Processing* 142: Art. ID.106747.

Ozer HO, Hacioglu Y and Yagiz N (2018) High order sliding mode control with estimation for vehicle active suspensions. *Transactions of the Institute of Measurement and Control* 40(5): 1457–1470.

Paul S, Yu W and Li X (2019) Discrete-time sliding mode for building structure bidirectional active vibration control. *Transactions of the Institute of Measurement and Control* 41(2): 433–446.

Peng J, Ding Y, Zhang G and Ding H (2020) Smoothness-oriented path optimization for robotic milling processes. *Science China Technological Sciences* 63(9): 1751–1763.

Poznyak A (2010) *Advanced mathematical tools for control engineers: volume 1: deterministic systems*. Elsevier.

Salgado I, Chairez I, Bandyopadhyay B, Fridman L and Camacho O (2014) Discrete-time non-linear state observer based on a super twisting-like algorithm. *IET Control Theory & Applications* 8(10): 803–812.

Shen W, Hu T, Zhang C, Ye Y and Li Z (2020) A welding task data model for intelligent process planning of robotic welding. *Robotics and Computer-Integrated Manufacturing* 64: 101934.

Spong M and Vidyasagar M (1989) *Robot dynamics and control*. John Wiley & Sons.

Su WC, Drakunov SV and Ozguner U (2000) An o (t/sup 2/) boundary layer in sliding mode for sampled-data systems. *IEEE Transactions on Automatic Control* 45(3): 482–485.

Tang Q, Li Y, Guo R, Jin D, Hong Y and Huang H (2021) Chattering-suppression sliding mode control of an autonomous underwater vehicle based on nonlinear disturbance observer and power function reaching law. *Transactions of the Institute of Measurement and Control* 43(9): 2081–2093.

Utkin V (1977) Variable structure systems with sliding modes. *IEEE Transactions on Automatic control* 22(2): 212–222.

Utkin V (2013) *Sliding modes in control and optimization*. Springer Science & Business Media.

Wang H, Li S, Lan Q, Zhao Z and Zhou X (2017) Continuous terminal sliding mode control with extended state observer for pmsm speed regulation system. *Transactions of the Institute of Measurement and Control* 39(8): 1195–1204.

Wang H, Pan Y, Li S and Yu H (2018) Robust sliding mode control for robots driven by compliant actuators. *IEEE Transactions on Control Systems Technology* 27(3): 1259–1266.

Wang Z, Li S and Li Q (2020) Discrete-time fast terminal sliding mode control design for DC–DC buck converters with mismatched disturbances. *IEEE Transactions on Industrial Informatics* 16(2): 1204–1213.

Xiao M, Ding Y and Yang G (2021) A model-based trajectory planning method for robotic polishing of complex surfaces. *IEEE Transactions on Automation Science and Engineering* 19(4): 2890–2903.

Yan Y, Wang XF, Marshall BJ, Liu C, Yang J and Chen WH (2023) Surviving disturbances: A predictive control framework with guaranteed safety. *Automatica* 158: 111238.

Yu X and Kaynak O (2009) Sliding-mode control with soft computing: A survey. *IEEE Transactions on Industrial Electronics* 56(9): 3275–3285.

Zhang J, Shi P, Xia Y and Yang H (2018) Discrete-time sliding mode control with disturbance rejection. *IEEE Transactions on Industrial Electronics* 66(10): 7967–7975.

Zhang J, Zhang N, Shen G and Xia Y (2019) Analysis and design of chattering-free discrete-time
    sliding mode control. *International Journal of Robust and Nonlinear Control* 29(18): 6572–
    6581.